# The global overturning circulation and the importance of non-equilibrium effects in ECCOv4r4

Tatsu Monkman[1] and Malte Friedrich Jansen[2]

[1]The University of Chicago
[2]University of Chicago

November 23, 2022

**Abstract**

We quantify the volume transport and watermass transformation rates of the global ocean circulation using the Estimating the Circulation and Climate of the Ocean version 4 release 4 (ECCOv4r4) reanalysis product. Our results support large rates of intercell exchange between the mid-depth and abyssal cells, in agreement with modern theory and observations. However, the present-day circulation in ECCO cannot be interpreted as a near-equilibrium solution. A dominant portion of the apparent diapycnal transport of watermasses within the deep ocean is not associated with irreversible watermass transformation. Instead up- and down-welling is associated with isopycnal volume changes, reflecting trends in the deep ocean density structure. Our results reveal disagreement between ECCO's representation of the overturning circulation and associated watermass transformations, and prevailing equilibrium theories of the overturning circulation.

# The global overturning circulation and the importance of non-equilibrium effects in ECCOv4r4

**Tatsu Monkman**[1] **and Malte F. Jansen**[1]

[1]The University of Chicago

**Key Points:**

- The MOC in ECCOv4r4 exhibits substantial linkage between the mid-depth and abyssal cells.
- Transient isopycnal volume change is prevalent in ECCO's deep ocean and plays a key role in the watermass budget of the MOC.
- ECCO's transient interior state must be taken into account when studying its climatological state.

Corresponding author: Tatsu Monkman, tdmonkman@uchicago.edu

**Abstract**

We quantify the volume transport and watermass transformation rates of the global ocean circulation using the Estimating the Circulation and Climate of the Ocean version 4 release 4 (ECCOv4r4) reanalysis product. Our results support large rates of intercell exchange between the mid-depth and abyssal cells, in agreement with modern theory and observations. However, the present-day circulation in ECCO cannot be interpreted as a near-equilibrium solution. A dominant portion of the apparent diapycnal transport of watermasses within the deep ocean is not associated with irreversible watermass transformation. Instead up- and down-welling is associated with isopycnal volume changes, reflecting trends in the deep ocean density structure. Our results reveal disagreement between ECCO's representation of the overturning circulation and associated watermass transformations, and prevailing equilibrium theories of the overturning circulation.

## Plain Language Summary

We analyze results taken from the Estimating the Circulation and Climate of the Ocean (ECCOv4r4) state estimate in order to investigate the internal structure and water mass budget of the global ocean's large-scale circulation. Our results support the modern view of an interconnected global ocean with substantial exchange between the overturning circulation of the Atlantic and that of the Indo-Pacific via the Southern Ocean. However, our investigation also reveals that the density structure of much of the deep ocean in the ECCO product is in a state of change, and that these changes play a key role in the watermass budget of the circulation. These results reveal disagreement between the model's representation of the deep ocean and the prevailing theoretical depictions of the ocean's large-scale circulation, which generally assume that the circulation is in a steady state.

## 1 Introduction

The global meridional overturning circulation (MOC) modulates the exchange of watermasses between the surface and the deep ocean and facilitates a large portion of the world's heat transport and carbon dioxide uptake (Toggweiler et al., 2006; Ferrari & Ferreira, 2011). The MOC is often described in terms of two circulation cells: the mid-depth cell, which is primarily located in the upper- and mid-depths of the Atlantic Ocean and is associated with the formation of North Atlantic Deep Water (NADW) via surface transformations in the north and wind-driven upwelling in the south (Marshall & Speer, 2012), and the abyssal cell, which occupies much of the deep and abyssal Indo-Pacific basin and is associated with Antarctic Bottom Water (AABW) formation off the coast of Antarctica (Gordon, 2001) and diffusive upwelling in the ocean interior (Weaver et al., 1999). Changes in either limb of the MOC could have a profound effect on both regional and global-scale climate (e.g. Zhang et al., 2019).

Despite the importance of the MOC to Earth's past and future climate, our understanding of the MOC's interior structure is incomplete. We still lack a clear consensus on the exchange rate of volume between the mid-depth and abyssal cells, and on the role and rates of diapycnal diffusion, which governs the interior watermass transformations thought to be critical to maintaining the MOC. Our incomplete understanding of the structure of the deep ocean circulation and the water mass transformations that govern it leads to uncertainty in predicting its role in future and past climate shifts, and serves as motivation for this study.

Our first objective is to study the return pathways of NADW and the amount of inter-cell coupling within the MOC in ECCOv4r4. Observational and theoretical evidence supports a large amount of exchange between the mid-depth and abyssal cells via the Southern Ocean, although there is some disagreement about the actual magnitude of ex-

change that occurs. Hydrographic analysis by Talley (2013) suggests that most NADW is converted to abyssal-cell AABW near the coast of Antarctica (≈13Sv), and re-circulates through the abyssal cell before returning into the Atlantic (c.f. Ferrari et al., 2014). Inverse analysis by Lumpkin and Speer (2007) shows a somewhat more even partitioning of NADW between the abyssal cell (≈11Sv) and recirculation within the mid-depth cell (≈7Sv), and a roughly similar partitioning is found by Cessi (2019) in the ECCOv4r2 state estimate (spanning 1992-2011). A recent study by Rousselet et al. (2021) uses Lagrangian drifters in ECCOv4r3 to find a similar partition of NADW between "upper" (32%) and "lower" (78%) recirculation routes, and argues that the lower route is further partitioned into an abyssal route through the Indo-Pacific (48%) and a "subpolar" cell route (20%) localized to the Southern Ocean. Here, we quantify the fate of NADW from a basin-wide net isopycnal volume budget perspective in ECCOv4r4, thus focusing on the overall strengths of the various circulation limbs, rather than the pathways taken by individual water parcels (as addressed by Rousselet et. al., 2021). In our study, inter-cell exchange is defined based on the amount of NADW that leaves the Atlantic below the isopycnal that separates the mid-depth and abyssal cells in the Southern Ocean (Nadeau et al., 2019). Since there is no net upwelling across this isopycnal in the Southern Ocean, this transport must be balanced by a similar amount of net upwelling in the Indo-Pacific.

Our second objective is to investigate the interior watermass transformations that maintain the MOC. Studies such as Gnanadesikan (1999), Wolfe and Cessi (2011) and (Nikurashin & Vallis, 2012) show that single-basin models with a southern re-entrant channel, where deep water formation in the north is balanced by wind-driven upwelling in the south, can recreate an adiabatic circulation that captures the major characteristics of the mid-depth cell (Lumpkin & Speer, 2007) - such an "adiabatic" mid-depth cell does not necessarily require any interior watermass transformations. The abyssal cell, meanwhile, is thought to be fundamentally governed by diabatic processes in the ocean interior, with negative surface buoyancy fluxes near the southern boundary balancing diffusive buoyancy gain and upwelling in the basin interiors to the north (Nikurashin & Vallis, 2012). In both cases the models hinge on the assumption that the circulation is in equilibrium, with diapycnal transport balanced exactly by irreversible watermass transformations, either via surface fluxes of heat and freshwater or via diapycnal mixing in the interior. We investigate the degree to which ECCOv4r4's MOC adheres to such circulation regimes and whether the common equilibrium assumption is valid when applied to the present-day ocean.

Our results support the general view of an interconnected global overturning circulation, as described in previous studies (e.g. Ferrari et al., 2017; Talley, 2013; Cessi, 2019). However, our results also reveal that ECCOv4r4's deep ocean is not in equilibrium and that isopycnal volume changes, associated with trends in the deep ocean density, play a key role in the interior circulation pathways.

## 2 Methods

### 2.1 The ECCOv4r4 State Estimate

We analyze monthly-mean results taken from the ECCOv4r4 ocean state estimate (Forget et al., 2015; ECCO Consortium et al., 2021, 2022). The ECCOv4 setup comprises a non-linear inverse modeling framework utilizing the MITgcm ocean model (Marshall et al., 1997) in conjunction with the adjoint method (Forget & Ponte, 2015) to produce an optimized solution of the hydrostatic Boussinesq equations fit to a suite of oceanographic data spanning the time period of 1992-2017 (ECCO Consortium et al., 2021). The model component of ECCOv4r4 uses the Lat-Lon-Cap 90 (LLC90) grid with a latitudinally-varying horizontal resolution between approximately 20km-40km at $80^o$N/S to 110km at $10^o$N/S. Further details about the ECCO state estimate are provided in Forget et al. (2015) and ECCO Consortium et al. (2021).

### 2.2 The Meridional Overturning Circulation in Potential Density Coordinates

We compute the isopycnal meridional overturning streamfunction, $\psi$, to evaluate the overall volume budgets of the global ocean circulation, subdivided by ocean basin. We perform our calculations in potential density space referenced to 2000dbar (henceforth $\sigma_2$), the approximate average local pressure of NADW within the Atlantic interior, which is consistent with Cessi (2019) and Rousselet et al. (2021). We compute the height of each isopycnal layer by linearly interpolating $\sigma_2$ values between depth levels, and compute transports by assuming vertically constant velocities within each grid box. This method is similar to that used by Ferrari and Ferreira (2011), and exactly conserves the vertically-integrated meridional mass transport at each grid point. The time-mean of $\psi$ as a function of $\sigma_2$ and latitude ($y$), $\psi(\sigma_2, y)$, is derived from the ECCOv4r4 diagnostic fields by vertically integrating the sum of the resolved meridional transport, $\mathbf{v}(x, y, z, t)$, and the parameterized meridional eddy transport, $\mathbf{v}^*(x, y, z, t)$, from the ocean bottom to a given $\sigma_2$ surface and then integrating zonally and averaging in time:

$$\psi(\sigma_2, y) = \overline{\int_{x_0(y)}^{x_1(y)} \int_{-H(x,y)}^{z(\sigma_2,x,y,t)} \mathbf{v}(x, y, z, t) + \mathbf{v}^*(x, y, z, t) dz dx}, \tag{1}$$

where $\int_{x_0(y)}^{x_1(y)} dx$ gives the zonal integral at a given latitude $y$ across an ocean basin bounded by longitudes $x_0$ and $x_1$. The overline denotes the time-average of the enclosed quantity over the full ECCO time period. $H(x, y)$ denotes the ocean depth and $z(\sigma_2, x, y, t)$ gives the depth of an isopycnal surface $\sigma_2$ at a particular location. We calculate $\psi$ by integrating across the Atlantic, Southern, and Indo-Pacific ocean basins, which in turn are divided by the continents and the $32^o$S parallel (Figure S1).

### 2.3 Volume Budget Decomposition in the Interior

We employ an isopycnal volume-budget analysis based on Walin (1982) to diagnose the processes that balance diapycnal advection within the large-scale circulation in ECCOv4r4. We consider a volume flux balance across the surface of an isopycnal volume of ocean, $V(\sigma_2, y_1, y_2)$, bounded above by an isopycnal of density $\sigma_2$, in the zonal direction by continental boundaries, and in the meridional by the latitudes , $y_1$, and $y_2$. For the Indo-Pacific and Atlantic $y_1 = 32^o$S, i.e. the northern edge of the Southern Ocean (Figure S1), and $y_2$ is the latitude where the isopycnal outcrops into the surface layer or the northern end of the basin. In the Southern Ocean we conversely set $y_2 = 32°$S, while $y_1$ is the latitude of the isopycnal outcrop. We define the bottom of the surface layer as the maximum surface potential density at or equatorwards of any given latitude over the entire ECCO period (i.e., the bottom of the surface layer as defined here is not itself a function of time). Following volume conservation, the total volume budget for an interior isopycnal volume can be expressed as:

$$\Delta\psi = \overline{\frac{d}{dt} V(\sigma_2, y_1, y_2, t)} + \overline{T_{geo}(\sigma_2, y_1, y_2, t)} + \overline{T_{mix}(\sigma_2, y_1, y_2, t)}. \tag{2}$$

Here $\Delta\psi = \overline{\psi(\sigma_2, y_2) - \psi(\sigma_2, y_1)}$ is the net transport across the northern and southern boundaries. $\overline{\frac{d}{dt} V(\sigma_2, y_1, y_2, t)}$ is the time-averaged change in the total volume itself (Newsom et al., 2016; de Lavergne et al., 2016):

$$\frac{d}{dt} V(\sigma_2, y_1, y_2, t) = \frac{d}{dt} \iint_{A_{\sigma_2}(y_1,y_2)} h(\sigma_2, x, y, t) dA, \tag{3}$$

where $h(\sigma_2, x, y, t)$ is the height of the isopycnal above the ocean bottom and $A_{\sigma_2}(y_1, y_2)$ is the isopycnal area bounded in the south and north by $y_1$ and $y_2$, respectively. $T_{geo}(\sigma_2, y_1, y_2, t)$ is the diapycnal transport due to geothermal heating:

$$T_{geo}(\sigma_2, y_1, y_2, t) = -\frac{\partial}{\partial \sigma_2} \iint_{A_I(\sigma_2, y_1, y_2, t)} \frac{\alpha Q_{geo}(x, y)}{c_p} dA, \tag{4}$$

where $A_I(\sigma_2, y_1, y_2, t)$ is the area where the bottom density $\sigma_{2b} \geq \sigma_2$ within the domain bounded by $y_1$, $y_2$ and the sides of the basin, $Q_{geo}(x, y)$ is the geothermal heat flux at the ocean floor, $\alpha = -\frac{1}{\sigma_2}\frac{\partial \sigma_2}{\partial \theta}$ is the thermal expansion coefficient, and $c_p$ is the heat capacity of seawater (see de Lavergne et al. (2016) for a full derivation). Numerically, the calculation of the transport associated with geothermal heating follows the same approach that is applied for surface transformations in Abernathey et al. (2016) (see also section S1 in the SI). $T_{mix}(\sigma_2, y_1, y_2, t)$ represents the watermass transformation rate due to mixing processes, which we compute as a residual of the other terms due to the difficulty in accounting for spurious diapycnal mixing associated with errors in the advection scheme (Griffies et al., 2000), parameterized mixing due to the Gaspar, Gregoris, and Lefevre (GGL) scheme (Gaspar et al., 1990), and horizontal mixing in the presence of slope-clipping along steep isopycnals[1]. This approach follows Newsom et al. (2016), Walin (1982), and Marsh et al. (2000). By applying (2) to specific domains of interest, we can estimate the major drivers of interior water mass transformations occurring within them. A schematic of our volume budget decomposition applied to the Atlantic, Indo-Pacific, and Southern Ocean basins is included in the supplement (Figure S2). For completeness, we also perform a similar volume budget decomposition for the surface layers in the Southern Ocean and North Atlantic, which is detailed in the SI.

## 3 Results

### 3.1 The isopycanl overturning in ECCO

The isopycnal overturning in ECCOv4r4 (Figure 1) is in broad agreement with that derived in other studies (e.g. Lumpkin & Speer, 2007; Cessi, 2019) and the magnitudes of the overturning cells generally fall within uncertainties established by observational estimates (Lumpkin and Speer (2007), Talley (2013), Kunze (2017)), as previously found for ECCOv4r2 by Cessi (2019). The mid-depth cell occupies the Atlantic with a peak overturning strength of 17.2Sv occurring at $55^o$N, in good agreement with other estimates (Lumpkin & Speer, 2007; Talley, 2013). The abyssal cell dominates the Indo-Pacific and the lower part of the Southern Ocean and peaks at approximately 14.4Sv at $36^o$S, a substantially weaker value than that derived by Lumpkin and Speer (2007) (20Sv), Talley (2013) (29Sv), and Kunze (2017) (20Sv), but similar to the estimates of de Lavergne et al. (2016) (10-15Sv). The abyssal cell in our analysis is also weaker than the value reported in Cessi (2019) (20Sv, at 30S), who employed ECCO version 4 release 2.

Large-scale diapycnal transport is visible in all ocean basins (Figure 1, Figure 3). In the Atlantic ≈3.0Sv of NADW upwell diabatically across the $\sigma_2$=1036.8kg/m$^3$ isopycnal and return to the surface in the North Atlantic (Figure 1a). Downwelling occurs in the lower range of NADW, yielding around 8.3Sv of transport at $\sigma_2$=1036.95kg/m$^3$ over the length of the Atlantic. The abyssal cell is almost entirely confined to the Indo-Pacific, where upwelling peaks at 14.4Sv at $\sigma_2 = 1037.053$kg/m$^3$.

[1] The MITgcm configuration used for ECCO employs a slope clipping that limits the effective isopycnal slope used in the Gent and Mcwilliams (1990) and Redi (1982) parameterizations to a maximum value of $2 \cdot 10^{-3}$. When this maximum slope is exceeded, mixing is no longer strictly isopycnal.

The net exchange of watermasses between the Atlantic's mid-depth cell and the abyssal cell can be found by considering the Atlantic, Indo-Pacific and Southern Ocean overturning stream functions at 32$^o$S. In ECCOv4r4, 14.2Sv of NADW exit the Atlantic at 32$^o$S, of which 4.6Sv enter the Southern Ocean at density classes occupied by the mid-depth cell ($\sigma_2 < 1036.95\text{kg/m}^3$). The lower 9.6Sv of NADW enter the Southern Ocean in the density range of the abyssal cell ($\sigma_2 \geq 1036.95\text{kg/m}^3$), and hence must be balanced by a similar amount of upwelling in the Indo-Pacific.

The natural question that arises next is how the diapycnal up- and down-welling in the interior of the Atlantic and Indo-Pacific basins is balanced by watermass transformations, which will be discussed in the following section.

### 3.2 Volume Budget Analysis

We consider the isopycnal volume budgets in the Atlantic, Indo-Pacific, and Southern Ocean interiors (Figure 2). In the Atlantic, net interior mixing-driven transformations amount to about 3.2Sv of upwelling at $\sigma_2 = 1036.74$ which corresponds to a depth range of around 1000-1500m, where a vertically increasing stratification is associated with buoyancy flux convergence (Munk, 1966). The diffusive upwelling accounts for most of the observed diapycnal upwelling in the North Atlantic at this depth range. The majority of the apparent diapycnal downwelling of lower NADW in the Atlantic instead is associated with the volume tendency term, $dV/dt$. The Atlantic net volume tendency peaks at $\sigma_2 = 1036.95\text{kg/m}^3$, contributing to a downwelling of -6.2Sv over the Atlantic basin. Notice that this downwelling is not associated with watermass transformation, but instead represents a downward advection of isopycnals over the course of the ECCOv4r4 time-span. This adiabatic downwelling is combined with a relatively small mixing-driven diapycnal downwelling ($T_{mix} \approx$-2Sv) at this depth to account for the time-mean downward transport of about -8.3Sv at $\sigma_2$=1036.95. As expected, geothermal heating is associated with diapycnal upwelling ($T_{geo}$) but is significant only for the densest watermasses below $\sigma_2$=1037.053, where dense isopycnals incrop at the bottom of the Atlantic and experience geothermal heating.

Upwelling in the Indo-Pacific is also primarily associated with isopycnal volume change. The volume tendency term, $dV/dt$, dominates the volume budget of the Indo-Pacific over much of the abyssal ocean, contributing to a net upwelling of 14.05Sv at $\sigma_2 = 1037.04\text{kg/m}^3$, which amounts to a significant shoaling of isopycnals over the ECCO timespan, and accounts for the majority of the abyssal cell upwelling at the $\sigma_2 = 1037.04\text{kg/m}^3$ isopycnal (Figure 1). The abyssal cell in ECCO is hence far out of balance, with the majority of the upwelling in the abyssal Pacific associated with upward advection of isopycnals rather than diapycnal transformations. The sign of the mixing-driven watermass transformation varies with depth, contributing a maximum net downward transfer of -3.3Sv at $\sigma_2 = 1037.04\text{kg/m}^3$ and a maximum upward transfer of 6.3Sv at $\sigma_2 = 1037.1\text{kg/m}^3$, indicating enhanced downward buoyancy flux due to diapycnal mixing between these two density values, although the mechanism behind this enhanced flux remains unclear to us. Watermass transformations due to geothermal heating peak at $\sigma_2 = 1037.04\text{kg/m}^3$ with a value of 3.6Sv, corresponding to buoyancy gain and transport across the $\sigma_2 = 1037.04\text{kg/m}^3$ isopycnal, which in-crops along geothermally-active regions in the Southeast Pacific.

Both mixing and volume tendency terms are significant in the Southern Ocean. Mixing-driven downwelling is dominant between $\sigma_2 = 1036.8\text{kg/m}^3$ and $\sigma_2 = 1037.1\text{kg/m}^3$, which stands in contrast to the relatively low mixing-driven downwelling rates in the northern basins and may be related to strong diapycnal mixing as a result of slope clipping

in the isopycnal mixing parameterization[2], which arises due to the relatively steep isopycnal slopes in the Southern Ocean. Substantial mixing-driven upwelling is seen between $\sigma_2 \approx 1037.1\text{kg/m}^3$ and $\sigma_2 =\approx 1037.2\text{kg/m}^3$, with a maximum value of 11.7Sv at $\sigma_2 =\approx 1037.14\text{kg/m}^3$. This mixing-driven watermass transformation is partially compensated by a downward movement of density surfaces, leaving a net upwelling of 8.9Sv. Mixing also plays a major role in balancing the volume budgets within the surface layer in the Southern Ocean (Figure S3), consistent with previous results for coarse-resolution ocean models (Newsom et al., 2016).

## 4 Summary and Discussion

Our results support an interconnected view of the MOC (summarized in Figure 3), with substantial linkages between the AMOC and the abyssal cell. It is clear that substantial diapycnal upwelling in the Indo-Pacific is needed to balance the inflow of dense NADW into the Southern Ocean. We also find significant up- and down-welling within the Atlantic, the latter of which is not typically included in idealized depictions of the mid-depth cell, and may reflect systematic errors in ECCO's representation of the deep ocean.

Trends in overall isopycnal volumes as calculated from yearly means and subdivided by basin (a, b), and spatial fields of time-averaged vertical isopycnal velocities, in meters per year, (d, e) for $\sigma_2$=1036.95kg/m$^3$ (top) and $\sigma_2$=1037.053kg/m$^3$ (bottom) over the ECCOv4r4 timespan (1992-2017). Striking linear trends are visible in the Atlantic and Indo-Pacific Oceans.

In both ocean basins, much of the net diapycnal up- and down-welling is balanced by isopycnal volume changes, rather than mixing-driven watermass transformations, as usually assumed in theoretical models. The associated isopycnal depth trends in ECCOv4r4 represent vertical isopycnal displacement velocities on the order of +/- 5-20 m/yr and persist over the entire ECCOv4r4 time span (Figure 4 a,b). These trends are present in all of the major ocean basins and are relatively horizontally homogeneous over the Atlantic and Indo-Pacific basins (Figure 4, d,e).

In the Atlantic, we see deepening isopycnals that correspond to an overall lightening of the deep ocean associated with warming temperatures and decreasing salinity (not shown), which is broadly consistent with previous studies such as Palmer et al. (2015), Desbruyères et al. (2017), and Zanna et al. (2019), although these studies rely on many of the same data sources as ECCOv4r4 and are accompanied by large uncertainties. An under-representation of dense water inflows across the GIS ridges in ECCOv4r4 may also lead to biases in deep Atlantic density trends by limiting the amount of dense water entering the Atlantic basin (Figure S3; Rossby et al. (2018); Lumpkin and Speer (2007); Lee et al. (2019); Tesdal and Haine (2020)), which may be compensated by sinking of NADW during its southward path in ECCOv4r4.

In the Indo-Pacific, meanwhile, we see isopycnal shoaling associated with a cooling of the abyssal ocean (c.f. Wunsch and Heimback (2014), Liang (2015)), which is in disagreement with previous observational studies that suggest broad warming in the Indo-Pacific such as Purkey and Johnson (2010). This isopycnal shoaling is a leading order term in the abyssal isopycnal volume budget in ECCO, where abyssal upwelling is balanced primarily by isopycnal shoaling as opposed to diapycnal mixing, as usually assumed in equilbrium theories such as Munk (1966) or Nikurashin and Vallis (2012). Unfortunately, as argued by Wunsch and Heimbach (2014), it is impossible to be sure whether these trends are the result of long-term trends in ocean climate, intrinsic ocean variabil-

[2] Analysis of isopycnal slopes in the abyssal Southern Ocean indicates that the slopes there frequently exceed the critical value that leads to slope clipping.

ity, or modeling and/or sampling biases. However, it is plausible that isopycnal shoaling in ECCO's deep Indo-Pacific is the result of an under-representation of diapycnal mixing in the abyssal ocean interior, leading to a mixing-driven transport that is too small to compensate for the in-flow of dense AABW. ECCO's background vertical diffusivity (Figure S4) appears to be multiple orders of magnitude lower than other contemporary estimates of abyssal mixing (de Lavergne et al., 2020).

The transient evolution of ECCOv4r4's deep ocean must be taken into account when interpreting ECCO results and comparing the circulation to theoretical models that are based on an equilibrium assumption. In the equilibrium view, deep water formation in the high latitudes must be balanced by wind-driven upwelling along isopycnals or irreversible processes in the ocean interior, which in turn are typically assumed to be dominated by diapycnal mixing (e.g. Nikurashin & Vallis, 2012; Marshall & Speer, 2012; Ferrari et al., 2017). Such a balance does not hold in ECCOv4r4, instead, the model depicts a global ocean in a transient state with regions of net warming (Atlantic), cooling (Indo-Pacific), and both (the deep Southern Ocean), where much of the interior up- and downwelling is not balanced by watermass transformations. If the ECCO solution is correct, prevailing equilibrium theories of the overturning circulation cannot be applied to the present-day ocean. However, at least some of the trends in ECCO are likely to be unrealistic, which would imply that ECCO's representation of the overturning circulation and watermass transformations are inconsistent. Regardless, the presence of isopycnal volume trends is important when interpreting ECCO's climatological mean state, as the assumption of an equilibrium state leads to apparent interior watermass transformations that are actually associated with trends in the watermass volumes.

**Acknowledgments**

This work was supported by the National Science Foundation through award OCE-1846821. The ECCO data are available in these in-text data citation references: ECCO Consortium et al. (2022). The ECCO data are publicly available at https://ecco-group.org/products.htm. The authors would like to thank Paola Cessi for providing her MATLAB scripts for the ECCO data analysis for comparison.

## References

Abernathey, R. P., Cerovecki, I., Holland, P. R., Newsom, E., Mazloff, M., & Talley, L. D. (2016). Water-mass transformation by sea ice in the upper branch of the southern ocean overturning. *Nature Geoscience*, *9*, 596–601. doi: 10.1038/NGEO2749

Cessi, P. (2019). The Global Overturning Circulation. *Annual Review of Marine Science*, *11*(1), 249-270. doi: 10.1146/annurev-marine-010318-095241

de Lavergne, C., Madec, G., Le Sommer, J., George Nurser, A. J., & Naveira Garabato, A. C. (2016). On the consumption of Antarctic Bottom Water in the abyssal ocean. *Journal of Physical Oceanography*, 635-661. doi: 10.1175/JPO-D-14-0201.1

de Lavergne, C., Vic, C., Madec, G., Roquet, F., Waterhouse, A. F., Whalen, C. B., ... Hibiya, T. (2020). A parameterization of local and remote tidal mixing. *Journal of Advances in Modeling Earth Systems*, *12*. doi: 10.1029/2020MS002065

Desbruyères, D. G., McDonagh, E. L., King, B. A., & Thierry, V. (2017). Global and Full-Depth Ocean Temperature Trends during the Early Twenty-First Century from Argo and Repeat Hydrography. *Journal of Climate*, *30*(6), 1985-1997. doi: 10.1002/2015GL067254

ECCO Consortium, Fukumori, I., Wang, O., Fenty, I., Forget, G., Heimbach, P., & Ponte, R. M. (2021). Synopsis of the ecco central production global ocean and sea-ice state estimate (version 4 release 4). *ECCO Consortium*. Retrieved from

https://doi.org/10.5281/zenodo.4533349

ECCO Consortium, Fukumori, I., Wang, O., Fenty, I., Forget, G., Heimbach, P., & Ponte, R. M. (2022). Ecco central estimate (version 4 release 4). *ECCO Consortium*. Retrieved from https://ecco.jpl.nasa.gov/drive/files/Version4/Release4/ (last accessed on 3/20/2022)

Ferrari, R., & Ferreira, D. (2011). What processes drive the ocean heat transport? *Ocean Modelling*, *38*(3-4), 171-186. doi: 10.1016/j.ocemod.2011.02.013

Ferrari, R., Jansen, M., Adkins, J., Burke, A., Stewart, A., & Thompson, A. (2014). Antarctic sea ice control on ocean circulation in present and glacial climates. *Proceedings of the National Academy of Sciences*, *111*(24), 8753-8758. doi: 10.1073/pnas.1323922111

Ferrari, R., Nadeau, L.-P., Marshall, D. P., Allison, L. C., & Johnson, H. L. (2017). A Model of the Ocean Circulation with Two Closed Basins and a Reentrant Channel. *Journal of Physical Oceanography*, *47*(12), 2887-2906. doi: 10.1175/JPO-D-16-0223.1

Forget, G., J.-M., C., Heimbach, P., Hill, C. N., Ponte, R. M., & Wunsch, C. (2015). ECCO version 4: an integrated framework for non-linear inverse modeling and global ocean state estimation. *Geoscientific Model Development*, *8*(10), 3071-3104. doi: 10.5194/gmd-8-3071-2015

Forget, G., & Ponte, R. (2015). The partition of regional sea level variability. *Progress in Oceanography*, *137*, 173-195. doi: 10.1016/j.pocean.2015.06.002

Gaspar, P., Grégoris, Y., & Lefevre, J.-M. (1990). A simple eddy kinetic energy model for simulations of the oceanic vertical mixing: Tests at station Papa and long-term upper ocean study site. *Journal of Geophysical Research: Oceans*, *95*(C9), 16179-16193. doi: 10.1029/JC095iC09p16179

Gent, P. R., & Mcwilliams, J. C. (1990). Isopycnal mixing in ocean circulation models. *Journal of Physical Oceanography*, *20*, 150–155. doi: 10.1175/1520-0485(1990)020⟨0150:IMIOCM⟩2.0.CO;2

Gnanadesikan, A. (1999). A simple predictive model for the structure of the oceanic pycnocline. *Science*, *283*(5410), 2077-2079. doi: 10.1126/science.283.5410.2077

Gordon, A. (2001). Bottom Water Formation. *Encyclopedia of Ocean Sciences (Second Edition)*. doi: 10.1016/B978-012374473-9.00006-0

Griffies, S. M., Pacanowski, R. C., & Hallberg, R. W. (2000). Spurious diapycnal mixing associated with advection in a z-coordinate ocean model. *Monthly Weather Review*, *128*, 538-564. doi: 10.1175/1520-0493(2000)128⟨0538:SDMAWA⟩2.0.CO;2

Kunze, E. (2017). The internal-wave-driven meridional overturning circulation. *Journal of Physical Oceanography*, 2673-2689. doi: 10.1175/JPO-D-16-0142.1

Lee, S.-K., Lumpkin, R., Baringer, M. O., Meinen, C. S., Goes, M., Dong, S., ... Yeager, S. G. (2019). Global Meridional Overturning Circulation Inferred From a Data-Constrained Ocean and Sea-Ice Model. *Geophysical Research Letters*, *46*(3), 1521-1530. doi: 10.1029/2018GL080940

Lumpkin, & Speer. (2007). Global Ocean Meridional Overturning. *Journal of Physical Oceanography*, *37*(10), 2550-2562. doi: 10.1175/JPO3130.1

Marsh, R., George Nurser, A. J., Megann, A. P., & New, A. L. (2000). Water mass transformation in the southern ocean of a global isopycnal coordinate gcm. *American Meteorological Society*, *30*, 1013-1045. doi: 10.1175/1520-0485(2000)030⟨1013:WMTITS⟩2.0.CO;2

Marshall, J., Hill, C., & Perelman, L. (1997). Hydrostatic, quasi-hydrostatic, and nonhydrostatic ocean modeling. *Journal of Geophysical Research: Oceans*, *102*(C3), 5733-5752. doi: 10.1029/96JC02776

Marshall, J., & Speer, K. (2012). Closure of the meridional overturning circulation through Southern Ocean upwelling. *Nature Geoscience*, *5*(3), 171-181. doi: 10.1038/ngeo1391

Munk, W. H. (1966). Abyssal recipes. *Deep Sea Research*, *13*, 707-730. doi: 10.1016/0011-7471(66)90602-4

Nadeau, L., Ferrari, R., & Jansen, M. F. (2019). Antarctic Sea Ice Control on the Depth of North Atlantic Deep Water. *Journal of Climate*, *32*(9), 2537-2551. doi: 10.1175/JCLI-D-18-0519.1

Newsom, E. R., Bitz, C. M., Bryan, F. O., Abernathey, R., & Gent, P. R. (2016). Southern Ocean Deep Circulation and Heat Uptake in a High-Resolution Climate Model. *Journal of Climate*, *29*(7), 2597-2619. doi: 10.1175/JCLI-D-15-0513.1

Nikurashin, & Vallis. (2012). A theory of deep stratification and overturning circulation in the ocean. *Journal of Physical Oceanography*, 485-502. doi: 10.1175/2010JPO4529.1

Palmer, M., Roberts, C., Balmaseda, M., Chang, Y.-S., Chepurin, G., Ferry, N., ... Xue, Y. (2015). Ocean heat content variability and change in an ensemble of ocean reanalysis. *Climate Dynamics*, *49*, 909-930. doi: 10.1007/s00382-015-2801-0

Redi, M. H. (1982). Oceanic isopycnal mixing by coordinate rotation. *Journal of Physical Oceanography*, *12*, 1154–1158. doi: 10.1175/1520-0485(1982)012⟨1154:OIMBCR⟩2.0.CO;2

Rossby, T., Flagg, C., Chafik, L., Harden, B., & Søiland, H. (2018). A Direct Estimate of Volume, Heat, and Freshwater Exchange Across the Greenland-Iceland-Faroe-Scotland Ridge. *Journal of Geophysical Research: Oceans*, *123*(10), 7139-7153. doi: 10.1029/2018JC014250

Rousselet, L., Cessi, P., & Forget, G. (2021). Coupling of the mid-depth and abyssal components of the global overturning circulation according to a state estimate. *Science Advances*, *7*(21). doi: 10.1126/sciadv.abf5478

Talley, L. (2013). Closure of the Global Overturning Circulation Through the Indian, Pacific, and Southern Oceans: Schematics and Transports. *Oceanography*, *26*(1), 80-97. doi: 10.5670/oceanog.2013.07

Tesdal, J.-E., & Haine, T. W. N. (2020). Dominant terms in the freshwater and heat budgets of the subpolar north atlantic ocean and nordic seas from 1992 to 2015. *Journal of Geophysical Research: Oceans*, *125*(10). doi: 10.1029/2020JC016435

Toggweiler, J., Russell, J. L., & Carson, S. R. (2006). Midlatitude westerlies, atmospheric CO2, and climate change during the ice ages. *Paleooceanography*, *21*(PA2005). doi: 10.1029/2005PA001154

Walin, G. (1982). On the relation between sea-surface heat flow and thermal circulation in the ocean. *Tellus*, *34*(2), 187-195. doi: 10.1111/j.2153-3490.1982.tb01806.x

Weaver, A. J., Bitz, C. M., Fanning, A. F., & Holland, M. M. (1999). THERMOHALINE CIRCULATION: High-Latitude Phenomena and the Difference Between the Pacific and Atlantic. *Annual Review of Earth and Planetary Sciences*, *27*, 231-285. doi: 10.1146/annurev.earth.27.1.231

Wolfe, & Cessi. (2011). The Adiabatic Pole-to-Pole Overturning Circulation. *Journal of Physical Oceanography*, *41*(9), 1795-1810. doi: 10.1175/2011JPO4570.1

Wunsch, C., & Heimbach, P. (2014). Bidecadal thermal changes in the abyssal ocean. *Journal of Physical Oceanography*, 2013-2030. doi: 10.1175/JPO-D-13-096.1

Zanna, L., Khatiwala, S., Gregory, J. M., Ison, J., & Heimbach, P. (2019). Global reconstruction of historical ocean heat storage and transport. *Proceedings of the National Academy of Sciences*, *116*(4), 1126-1131. doi: 10.1073/pnas.1808838115

Zhang, R., Sutton, R., Gokhan, D., Young-Oh, K., Marsh, R., Yeager, S. G., ... Little, C. M. (2019). A Review of the Role of the Atlantic Meridional Overturning Circulation in Atlantic Multidecadal Variability and Associated Climate

Impacts. *Reviews of Geophysics*, *57*(2), 316-375. doi: 10.1029/2019RG000644

# The global overturning circulation and the importance of non-equilibrium effects in ECCOv4r4 FIGURES

**Tatsu Monkman**[1] **and Malte F. Jansen**[1]

[1]The University of Chicago

Corresponding author: Tatsu Monkman, tdmonkman@uchicago.edu

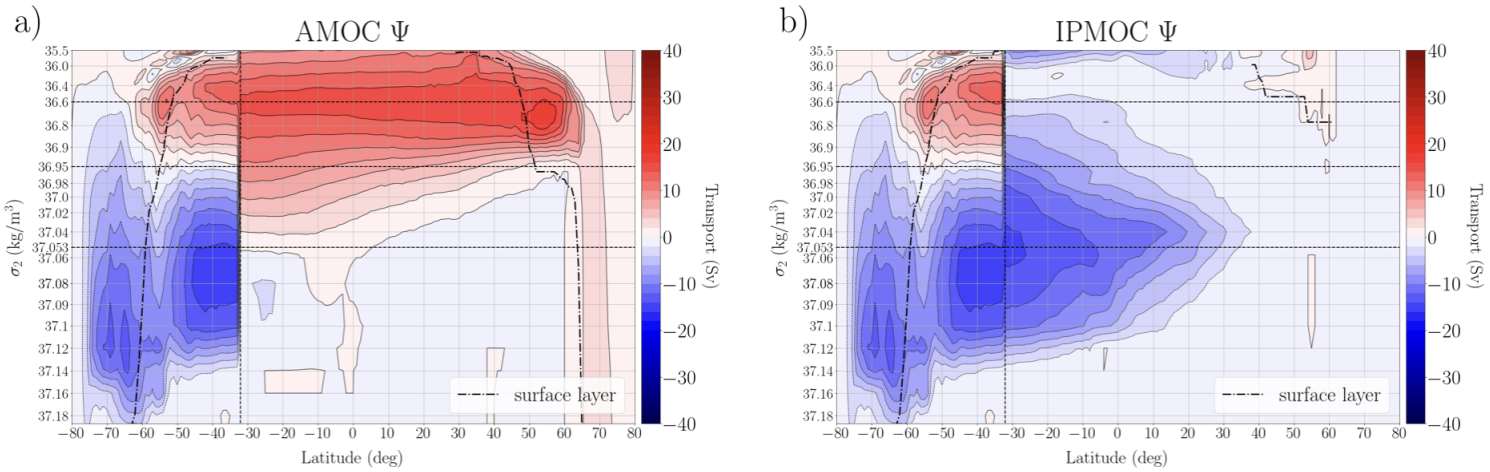


**Figure 1.** Atlantic, Indo-Pacific, and Southern Ocean stream functions in potential density space (referenced to 2000dbar), calculated from ECCOv4r4 and averaged over the full ECCO time period (1992-2017). (a) the Atlantic Meridional Overturning Circulation (AMOC) and (b) Indo-Pacific Meridional Overturning Circulation (IPMOC). The Southern Ocean Meridional Overturning Circulation is plotted in both (a) and (b) south of 32°S. Positive (red) denotes clockwise flow and negative (blue) denotes counterclockwise flow (CL=2Sv). The dash-dotted line indicates the bottom of the surface layer (see text). The vertical dashed line indicates the northern end of the Southern Ocean at 32°S. Horizontal dashed lines denote specific density surfaces of interest: the upper bound of southward-flowing NADW: $\sigma_2$=1036.6kg/m$^3$, the division between the upper and lower cells in the Southern Ocean: $\sigma_2$=1036.95kg/m$^3$, and the maximum density of NADW entering the SO: $\sigma_2$=1037.05kg/m$^3$. The density-axis is stretched to reflect the average isopycnal depth within the Atlantic for $\sigma_2$<1037.1kg/m$^3$ (the maximum density in the Atlantic) and is extended linearly to the highest densities in the Southern Ocean. The same density axis is used in subsequent plots.

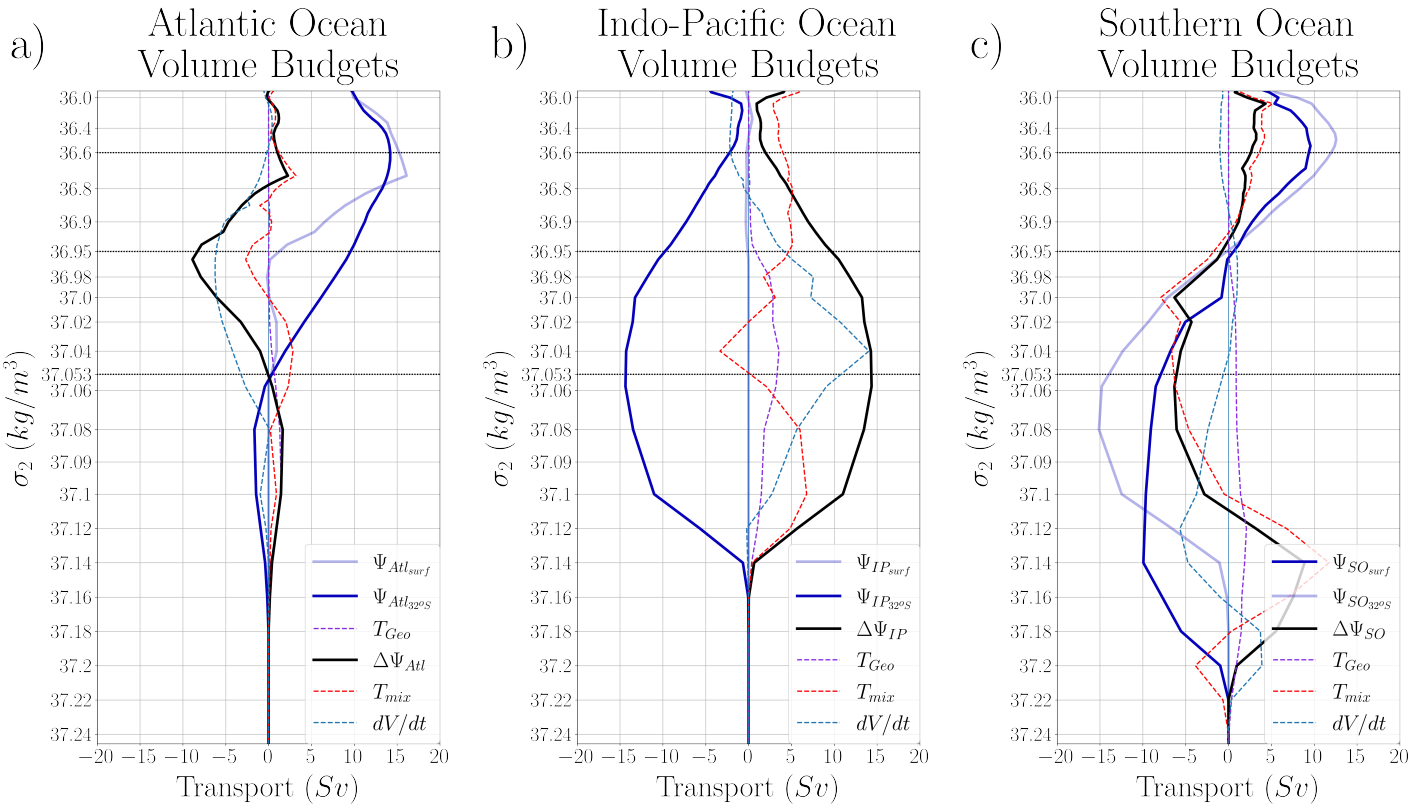


**Figure 2.** Volume budget decompositions across the Atlantic Ocean (**a**), Indo-Pacific Ocean (**b**), and Southern Ocean (**c**). Solid black lines denote net diapycnal transformation across density surfaces, inferred from the difference between $\Psi(\sigma_2)$ across each region's northern (light blue) and southern (dark blue) boundaries. The subscript $Surf$ refers to the stream function at the bottom of the surface layer, defined by the minimum surface density at a given latitude (Figure 1). The net diapycnal transport (solid black) is de-composed into contributions from: geothermal transformations (dashed purple), diffusive transformations (dashed red), and isopycnal volume change (dashed cyan).

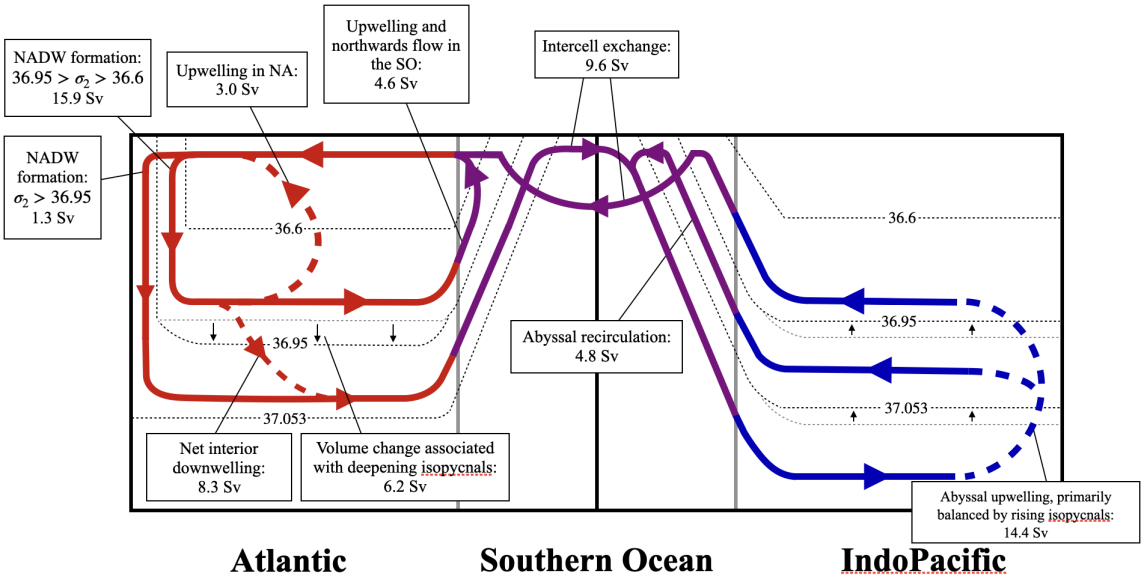


**Figure 3.** Schematic representation of the overturning, inferred from the stream function and volume budget decomposition (Figure 1, Figure 2). Net transport within the Atlantic Ocean (red arrows), Southern Ocean (purple arrows), and Indo-Pacific Ocean (blue arrows), are shown. Arrows denote direction of flow. Solid and dashed arrows below the surface denote primarily along- and across-isopycnal pathways, respectively. Dashed black lines denote the specific densities discussed in Figure 1, and isopycnal depth changes are indicated where they are the dominant contributor balancing up- and down-welling.

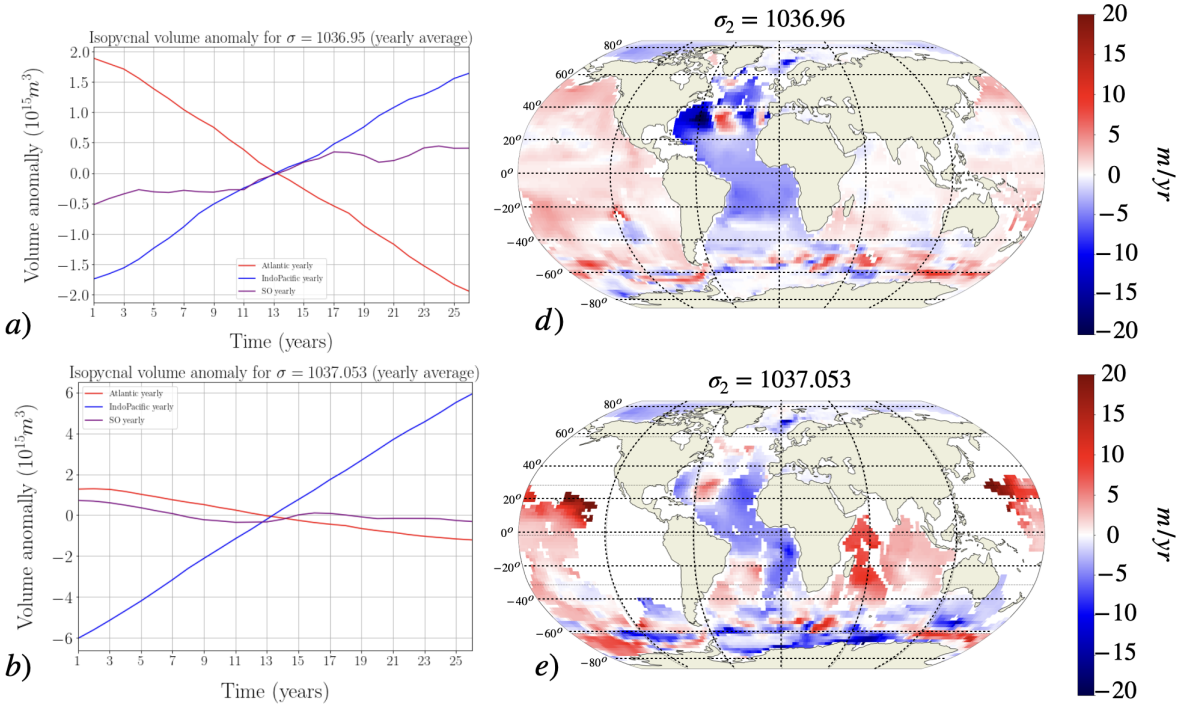


**Figure 4.** Trends in overall isopycnal volumes as calculated from yearly means and subdivided by basin (a, b), and spatial fields of time-averaged vertical isopycnal velocities, in meters per year, (d, e) for $\sigma_2$=1036.95kg/m$^3$ (top) and $\sigma_2$=1037.053kg/m$^3$ (bottom) over the ECCOv4r4 timespan (1992-2017). Striking linear trends are visible in the Atlantic and Indo-Pacific Oceans.

# Supporting Information for "The global overturning circulation and the importance of non-equilibrium effects in ECCOv4r3"

Tatsu Monkman[1]and Malte F. Jansen[1]

[1]University of Chicago

## Contents of this file

1. Text S1
2. Figures S1 to S4

## Introduction

The supporting information contains one text section and 3 figures supporting the results presented in our main text. Text section S1 outlines the calculations used to derive the volume budget and water-mass transformations in the surface layer. Figure S1 shows the domain masks used to define the major ocean basins in our study. Figure S2 gives a schematic representation of the various terms in the volume-budget presented in Figure 2 of the main text. Figure S3 shows the surface layer transformations in the Southern Ocean and the North Atlantic.

## S1. Calculation of Surface Layer Watermass Budgets in ECCOv4r3

Ultimately, any diapycnal transport in the surface layer must be balanced by buoyancy exchange with the atmosphere and/or sea ice and mixing. We perform a volume budget decomposition within the surface layer, which is analog to the interior volume budget decomposition described in the main text. Analog to the interior volume budget discussed in the main text, we assume that the volume transport at the base of the surface layer, $\psi_{surf}$ (minus the transport across the Greenland-Iceland-Scotland (GIS) ridge system, $\Psi_{GIS}$, in the case of the North Atlantic), must be balanced by heat- and freshwater-driven surface transformations, $T_{surf} = T_\Theta + T_S$, isopycnal volume change within the surface mixed layer, $\frac{d}{dt}V_{surf}$, and horizontal and vertical mixing, $T_{mix}$:

$$\overline{\Delta\psi(\sigma_2,t)} = \overline{\frac{d}{dt}V_{surf}(\sigma_2,t)} + \overline{T_{surf}(\sigma_2,t)} + \overline{T_{mix}(\sigma_2,t)}, \tag{S.1}$$

where all terms are defined as positive towards higher buoyancy (lower density). Here $\Delta\psi = \psi_{GIS} - \psi_{surf}$ in the North Atlantic and $\Delta\psi = \psi_{surf}$ in the Southern Ocean. We compute $\frac{d}{dt}V_{surf}(\sigma_2,t)$ as in the main text, this time including only volume changes that occur within the surface layer. We compute diapycnal transport associated with heat- and freshwater-driven surface density forcing, $T_\Theta$ and $T_S$, as in Newsom, Bitz, Bryan, Abernathey, and Gent (2016):

$$\begin{aligned} T_\Theta(\sigma_2,t) &= -\frac{\partial}{\partial\sigma_2}\iint_{A_O(\sigma_2,y_1,y_2,t)} \frac{\alpha}{c_p}Q_{surf}(x,y,t)dA \\ T_S(\sigma_2,t) &= -\frac{\partial}{\partial\sigma_2}\iint_{A_O(\sigma_2,y_1,y_2,t)} \frac{\rho_0}{\rho_{fw}}\beta S_0 f_{fw}(x,y,t)dA \end{aligned} \tag{S.2}$$

where the integration area, $A_O(\sigma_2,y_1,y_2,t)$, is the outcropping region where the surface potential density is larger than $\sigma_2$ within the particular basin of interest (in this case the

Southern Ocean and the North Atlantic), $Q_{surf}$ is the surface heat flux and $f_{fw}$ is the surface freshwater flux. $\alpha = -\frac{1}{\sigma_2}\frac{\partial \sigma_2}{\partial \Theta}$ and $\beta = \frac{1}{\sigma_2}\frac{\partial \sigma_2}{\partial S}$ are the thermal expansion and haline contraction coefficients, respectively, $c_p = 3994\text{J/kg/K}$ is the heat capacity of seawater, $\rho_0 = 1029.\text{kg/m}^3$ is the reference seawater density in ECCO, $\rho_{fw} = 1000.\text{kg/m}^3$ is the reference density of freshwater in ECCO, and $S_0 = 35\text{g/kg}$ is a reference salinity. Here we define the heat- and freshwater-driven transformation rates, $T_\Theta(\sigma_2, t)$ and $T_S(\sigma_2, t)$, as positive for transport towards lower densities. In the North Atlantic, we calculate the rate of deep water inflow across the GIS ridge system, $\Psi_{GIS}(\sigma, t)$, by measuring the rate of meridional transport across the northern boundary of the integration area. We denote the effect of horizontal and vertical diabatic mixing within the surface layer as $T_{mix}$, and calculate it as the residual of the time-means of the other terms in equation (S1).

The numerical implementation of the surface transformation terms follow that used by Abernathey et al. (2016) and is evaluated by discretizing $\sigma_2$ into evenly spaced bins at $\Delta\sigma_2 = 0.02\text{kg/m}^{-3}$ spacing. Equations (S2) are then evaluated numerically as

$$\begin{aligned} T_\Theta(\sigma_2, t) &= \frac{1}{\Delta\sigma_2}\sum_{i=1}^{N_x}\sum_{j=1}^{N_y} A_{c_{ij}}\frac{\alpha}{c_p}\, Q_{surf}\, \delta(\sigma_2 - \sigma_2') \\ T_S(\sigma_2, t) &= \frac{1}{\Delta\sigma_2}\sum_{i=1}^{N_x}\sum_{j=1}^{N_y} A_{c_{ij}}\frac{\rho_0}{\rho_{fw}}\beta S_0\, f_{fw}\, \delta(\sigma_2 - \sigma_2') \end{aligned} \tag{S.3}$$

where $A_c$ is the horizontal area of each grid cell and $N_x$ and $N_y$ are the zonal and meridional extents of the model domain. The discrete delta function, $\delta(\sigma_2 - \sigma_2')$, is defined as

$$\delta(\sigma_2 - \sigma_2') = \begin{cases} 1 & \text{if } (\sigma_2 - \Delta\sigma_2/2) <= \sigma_2' < (\sigma_2 + \Delta\sigma_2/2) \\ 0 & \text{else} \end{cases} \tag{S.4}$$

## References

Abernathey, R. P., Cerovecki, I., Holland, P. R., Newsom, E., Mazloff, M., & Talley, L. D. (2016). Water-mass transformation by sea ice in the upper branch of the southern ocean overturning. *Nature Geoscience*, *9*, 596–601. doi: 10.1038/NGEO2749

Newsom, E. R., Bitz, C. M., Bryan, F. O., Abernathey, R., & Gent, P. R. (2016). Southern Ocean Deep Circulation and Heat Uptake in a High-Resolution Climate Model. *Journal of Climate*, *29*(7), 2597-2619. doi: 10.1175/JCLI-D-15-0513.1

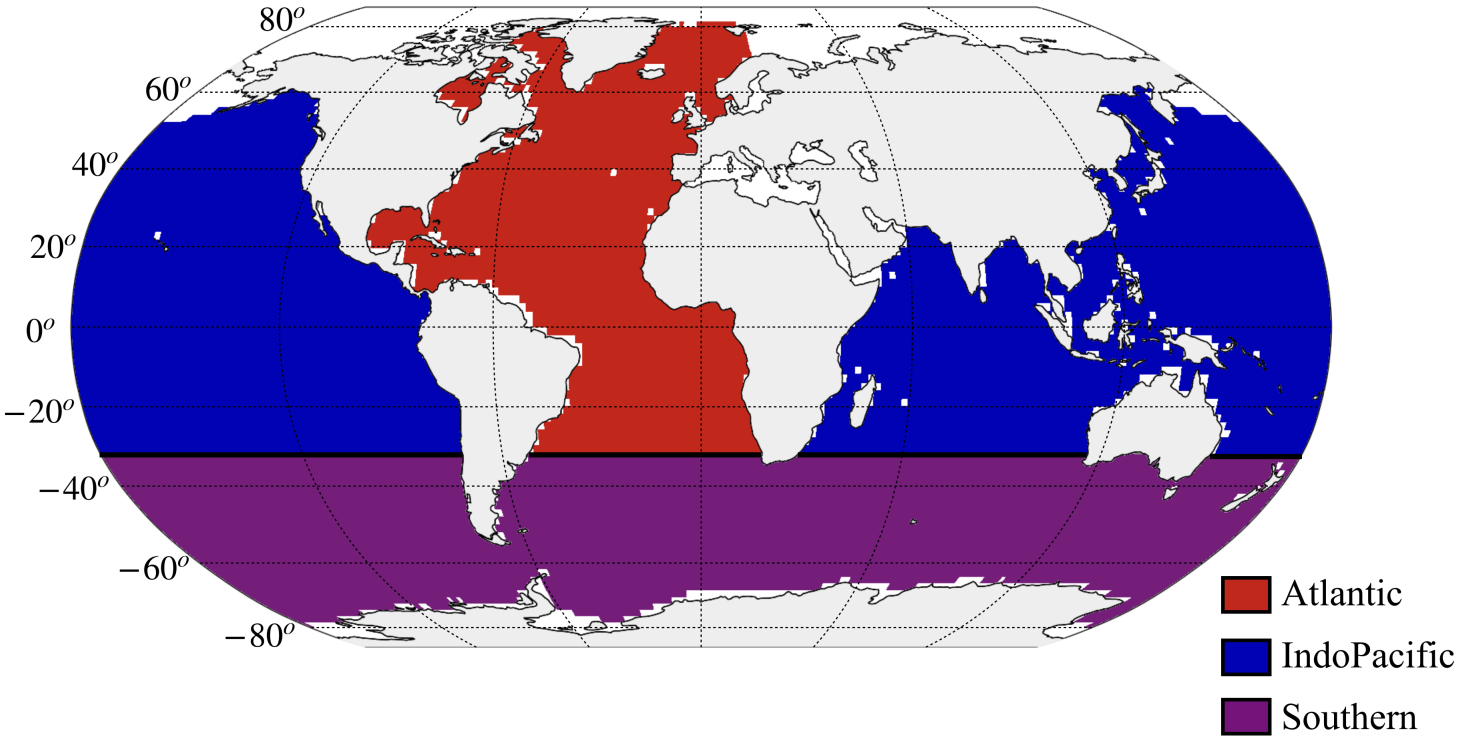


**Figure S1.** Basin masks used for subdividing the global ocean. The Atlantic basin (red) extends from $32^oS$ north into the Norwegian and Greenland seas. The Indo-Pacific basins (blue) are considered together and extend from $32^oS$ to the Aleutians in the North. The Southern Ocean (purple) is bounded in the north at $32^oS$ and extends to the coast of Antarctica.

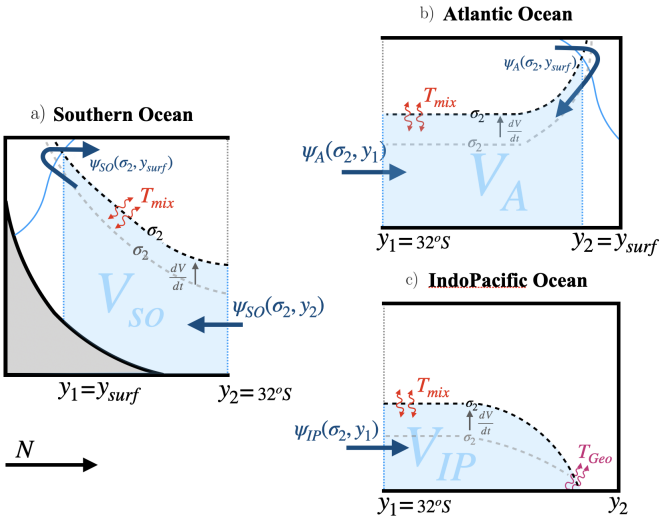


**Figure S2.** Schematic of the water-mass-transformation framework used in this study, applied to the Atlantic (subscript A), Indo-Pacific (subscript IP), and Southern Ocean (subscript SO). Black dashed lines indicate an isopycnal surface of density $\sigma_2$. Transports into and out of isopycnal volumes are indicated by arrows, with dark blue indicating advective flux ($\psi(\sigma_2, y)$), red diffusive flux ($T_{mix}$), grey apparent flux balanced by volume change ($dV/dt$), and purple transport balancing geothermal heating ($T_{Geo}$). Latitudes defining the southern and northern meridional bounds of the ocean basins are given by dotted blue lines and labeled $y_1$ and $y_2$, respectively, and the latitude where the isopycnal intersects with the surface layer is given by $y_{surf}$. The bottom of the surface layer is indicated by solid blue lines.

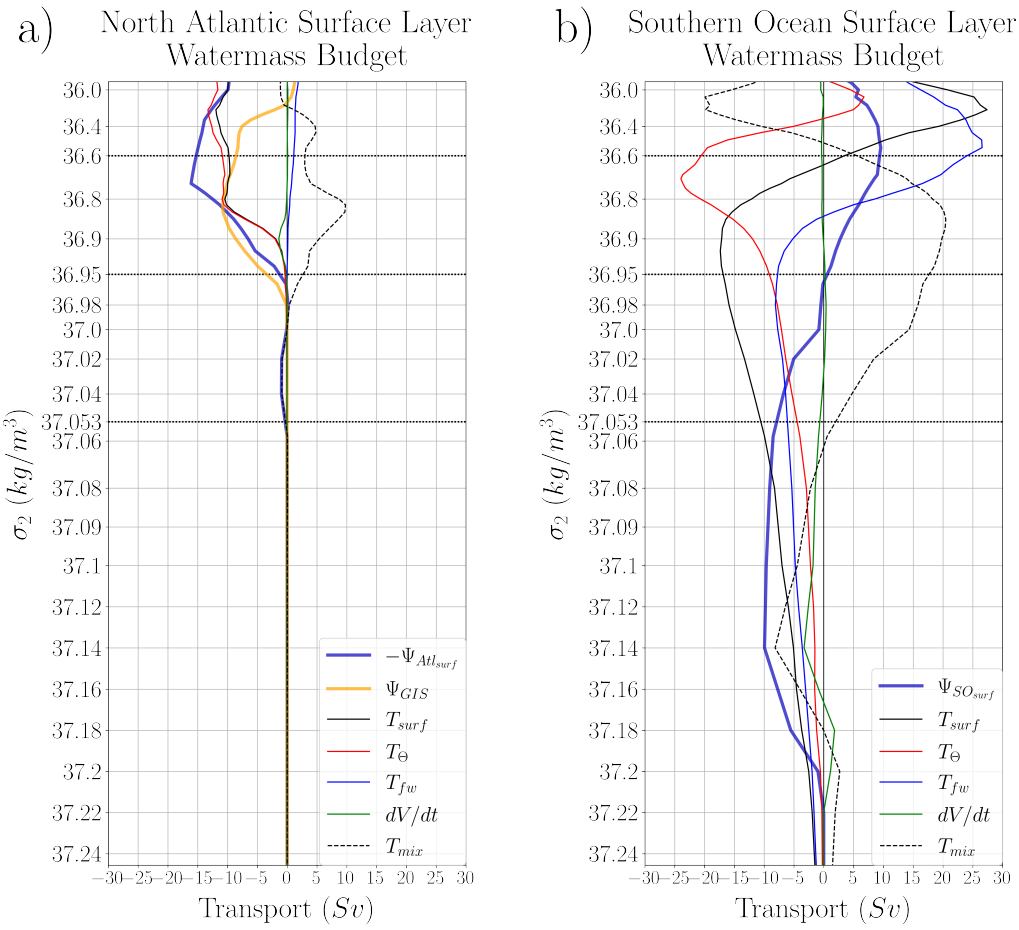


**Figure S3.** Water-mass-transformation decompositions in the surface layers of the North Atlantic (**a**) and Southern Ocean (**b**) high latitudes. All terms are defined positive for transformations towards higher buoyancy (lower density). Shown are the total surface transformation rate, $T_{surf}$, (thin, solid black) and its heat-driven, $T_\Theta$, (thin, solid red) and freshwater-driven, $T_{fw}$, (thin, solid blue) components, as well as contributions from isopycnal volume change within the surface layer, $dV/dt$, (thin, solid green). Dense water inflow across the Greenland-Iceland-Scotland (GIS) ridge system, $\Psi_{GIS}$, is included in (**a**) (thick, solid orange). Stream function values at the bottom of the surface layer (thick, solid blue) are shown in the North Atlantic, $-\Psi_{Atl_{surf}}$, and the Southern Ocean, $\Psi_{SO_{surf}}$. Note the sign of stream function values in the North Atlantic is flipped such that negative values denote transport towards higher density. Any contributions from surface-layer mixing are calculated as a residual, $T_{mix}$, (dashed, black).

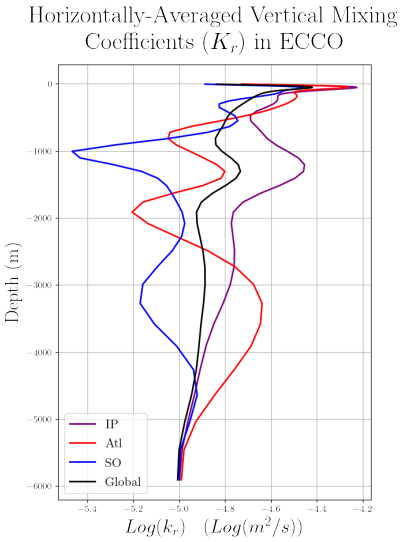


**Figure S4.** Vertical diffusivities $k_r$ $(m^2/s)$ in ECCOv4r3 horizontally averaged over the major ocean basins. Notice that these are the "background" diffusivities optimized by the inversion, and do not include mixing parameterized via the GGL scheme (diagnostics for which are not available). The averages presented are area-weighted horizontal averages, and masked using the same spatial mask as in Figure S1. Colored lines refer to the Indo-Pacific (purple), Atlantic (red), and Southern Ocean (blue). The black line gives the global average.